Reflectance measurements on clean surfaces for the determination of optical constants of silicon in the extreme ultraviolet–soft-x-ray region

Regina Soufli and Eric M. Gullikson

The refractive index $n = 1 - \delta + i\beta$ of Si in the energy range 50–180 eV is investigated with angle-dependent reflectance measurements. The optical constants δ and β are both determined by fitting to the Fresnel equations. The results of this method are compared with the values in the atomic tables derived from experimental data for β and implementation of the Kramers–Kronig relations for δ. The samples were prepared by UV irradiation and HF:ethanol dipping to H passivate the surface. It is found that the values of δ in the atomic tables are 8–15% too high in the region 50–90 eV. This is attributed to missing oscillator strength in the tabulated absorption coefficient for Si. The measured values of β for crystalline Si exhibit structure below the $L_{2,3}$ edge (99.8 eV), as was previously observed in transmission measurements of Si(111). It is also found that the method of least-squares fitting reflectance data to obtain optical constants is most effective for energies well below the edge, where $\delta > \beta$, while for a range of energies around and above the edge, where $\delta < \beta$, the optical constants are determined with large uncertainties. This behavior is not unique to the Si $L_{2,3}$ edge.

1. Introduction

The response of a given material to an incident electromagnetic wave is described by the energy-dependent complex index of refraction $n = 1 - \delta + i\beta$. In the extreme ultraviolet (EUV)–soft-x-ray spectral region, the need for accurate determination of n is driven by activity in areas such as synchrotron-based research, EUV–x-ray lithography, x-ray astronomy, and plasma applications. Knowledge of the refractive index is essential for the design of the optical components of instruments used in experiments and applications. Moreover, measured values of n can be used to evaluate solid-state models for the optical behavior of materials.

Various methods are used to determine the optical constants δ and β, such as reflectance measurements, angle-dependent electron yield, transmission measurements, interferometry, and ellipsometry. A comprehensive compilation of available experimental data on the optical constants was performed by Henke *et al.*[1] The absorption coefficient was deduced from both transmission measurements and theoretical calculations. The real part of n was then calculated through the Kramers–Kronig relations.

In this work the method of angle-dependent reflectance is evaluated and implemented to yield the optical constants of Si in the region around the $L_{2,3}$ edge (99.8 eV). The refractive index of Si in this energy range was investigated by previous experimenters[2,3,4] using various methods. The discrepancies among their data arise mainly owing to the surface quality of the samples used for measurements and the inherent difficulties of each method. Angle-dependent reflectance measurements have the advantage that both δ and β can be deduced experimentally, and thus provide an important test of the tabulated values of δ generated by the Kramers–Kronig relations. In addition, measurements can be performed on bulk samples without the need to fabricate the free-standing thin films required for transmission measurements. In this case the reflectance method has allowed measurements to be performed on amorphous Si when the high stress in sputtered films made the fabrication of free-standing films difficult. Some of the possible pitfalls of the method include its sensitivity to surface roughness and contamination.

R. Soufli is with the Department of Electrical Engineering and Computer Sciences, University of California at Berkeley, Berkeley, California 94720. R. Soufli and E. M. Gullikson are with the Center for X-ray Optics, Materials Sciences Division, Lawrence Berkeley National Laboratory, Berkeley, California 94720.

Received 3 June 1996; revised manuscript received 24 October 1996.

0003-6935/97/225499-09$10.00/0

Owing to its implementation as filter and spacer material in multilayer mirrors, Si is among the materials of particular importance for practical applications in the EUV–soft-x-ray range for energies below the $L_{2,3}$ edge. The choice of Si as the material for this study was also motivated by the ability to obtain highly polished wafers, thus reducing the effects of surface roughness, and the possibility of chemically cleaning and passivating the surface against oxidation. The cleaning treatment aiming at H passivation of the surface is described in Subsection 3.A. Reflectance data were obtained with two reflectometers, one with a laser-produced-plasma source and a second located at beamline 6.3.2 at the Advanced Light Source (ALS). The reflectometers are outlined in Subsection 3.B. A least-squares fitting algorithm with the Fresnel equations determines δ and β from the experimental reflectance curves, and the χ^2 distribution criterion is used to evaluate the reliability of the fitting results at different energies, as shown in Subsection 4.A. In Subsection 4.B the results are used to evaluate the accuracy of the tabulated optical constants determined by the Kramers–Kronig method.

2. Optical Constants from Theory and Experiment

It is common to write the frequency-dependent index of refraction $n(\omega)$ of a material in the form $n(\omega) = 1 - \delta + i\beta$. The quantities δ and β are the optical constants and are characteristic of a certain medium with a wave propagating at frequency ω. The electromagnetic wave propagation in a medium may also be considered a scattering process, in which the incident wave interferes with the sum of all forwardscattered radiation from the atoms of the material to produce a modified propagating wave. In the atomic description the following assumptions are made: (i) The photon energy is sufficiently low that coherent scattering and photoabsorption are the primary interactions of radiation with matter. (ii) The individual atoms scatter independently, i.e., unaffected by the condensed state of the system; this is approximately true for energies above ~50 eV and sufficiently outside the absorption threshold regions. In this case, the total coherently scattered amplitude is the vector sum of the amplitudes scattered by the individual atoms. The atomic scattering factor $f(\theta, \omega) = f_1(\theta, \omega) - if_2(\theta, \omega)$ may be introduced, where 2θ is the scattering angle; f represents the factor by which one must multiply the amplitude scattered by a single free electron to obtain the total amplitude coherently scattered by the particular atom. For wavelengths that are long compared with the atomic dimensions or for small scattering angles (when the scattering amplitudes are in phase), the atoms scatter as dipoles. The atomic scattering factor then becomes independent of the angle of scattering and equal to the forward ($\theta \simeq 0$) atomic scattering factor, $f = f(\omega) = f_1(\omega) - if_2(\omega)$. In this limit, if an optical electromagnetic description is applied, the complex refractive index n can be related to the forward atomic scattering factor f of the individual atoms of a certain material, as follows:

$$n = 1 - \delta + i\beta \simeq 1 - \frac{r_0}{2\pi}\lambda^2 n_a f, \tag{1}$$

where $r_0 = e^2/4\pi\epsilon_0 mc^2$ is the classical electron radius, λ is the wavelength of the radiation and n_a is the atomic density of the material. Thus, the optical constants δ and β are related to the real and the imaginary part f_1 and f_2 of the atomic scattering factor in the following manner:

$$\delta \simeq \frac{r_0}{2\pi}\lambda^2 n_a f_1, \tag{2}$$

$$\beta \simeq \frac{r_0}{2\pi}\lambda^2 n_a f_2. \tag{3}$$

Optical constants may be determined from absorption data with the Kramers–Kronig relations; f_2 is determined experimentally in the whole energy spectrum (e.g., from transmission measurements) and f_1 is obtained at any frequency ω with the x-ray form of the Kramers–Kronig relations:

$$f_1(\omega) - Z = -\frac{2}{\pi}\int_0^\infty \frac{uf_2(u)}{u^2 - \omega^2}\,du, \tag{4}$$

where Z is the atomic number of the element. The forward atomic scattering factors have been tabulated[1] by the above procedure for all elements from hydrogen ($Z = 1$) to uranium ($Z = 92$), across the energy range 30–30,000 eV. Equation (4) requires accurate experimental knowledge of f_2 in the whole range of frequencies to determine f_1 correctly at a frequency ω.

The accuracy of the experimental data for f_2 may be examined by means of the sum rule

$$Z = \frac{2}{\pi}\int_0^\infty \frac{f_2(u)}{u}\,du, \tag{5}$$

where $f_2(u)/u$ is the oscillator strength associated with the frequency u in the region $(0, \infty)$. In the case of materials with absorption thresholds well separated in energy so that the oscillator strength of one absorption region is exhausted before the onset of the next, a partial sum rule may be useful:

$$Z - \frac{2}{\pi}\int_\omega^\infty \frac{f_2(u)}{u}\,du = N_{\text{eff}}(\omega), \tag{6}$$

where $N_{\text{eff}}(\omega)$ represents the effective number of electrons in the atom contributing to the absorption, i.e., having binding energy less than the photon energy $\hbar\omega$. Thus, Eq. (6) guarantees that at high energies $N_{\text{eff}} = Z$. As the energy goes to zero, N_{eff} should also go to zero, if f_2 satisfies the sum rule of Eq. (5). Figure 1 shows a plot of $N_{\text{eff}}(\omega)$ for Si from the experimental data for f_2 from the atomic tables.[1] It is seen that the experimental $N_{\text{eff}}(\omega)$ is greater than

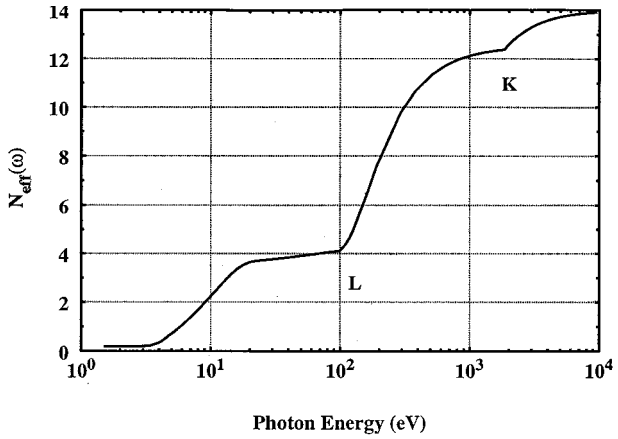

Fig. 1. Calculation of the left-hand side of the partial sum rule, Eq. (6), with the data for f_2 from Ref. 1. Although Eq. (6) requires that $N_{\text{eff}}(\hbar\omega \to 0) = 0$, the calculation with experimental data gives $N_{\text{eff}}(\hbar\omega \to 0) = 0.2$. This missing oscillator strength should cause overestimation of δ at low energies.

zero as $\hbar\omega$ goes to zero. This implies, from Eq. (6), that there is missing oscillator strength in the absorption spectrum.

One may ask, What effect will this missing oscillator strength have on the calculated values of f_1? The x-ray form of the Kramers–Kronig relation, Eq. (4), has the property that it yields the correct result ($f_1 = Z$) in the high-energy limit. Moreover, it can be shown[5] that if a defect in the data for the oscillator strength occurs around a frequency ω_d, then the values of f_1 determined with Eq. (4) will be correct in the region $\omega > \omega_d$, and Eq. (4) will overestimate f_1 for $\omega < \omega_d$. Because the deficiency in oscillator strength in the data for Si as shown in Fig. 1 is expected to lead to systematic errors in the determination of f_1 at low energies, it is particularly important to have an independent measurement such as provided by the reflectance method. In addition, in the $L_{2,3}$ absorption threshold energy region where fine structure is present, it would be interesting to obtain both real and imaginary parts of the refractive index n for silicon in an exclusively experimental manner.

3. Experiment

A. Sample Preparation

The samples used in this experiment were (1) Si(111) wafers, prime grade, n-doped with 10^{19} As atoms cm^{-3}, with resistivity $\rho = 0.005 - 0.013\ \Omega$ cm and thickness 330–530 μm; (2) Si(100) wafers, prime grade, n-doped with 10^{15} P atoms cm^{-3}, with resistivity $\rho = 3 - 7\ \Omega$ cm and thickness 356–406 μm; and (3) amorphous Si (3000 Å of sputtered Si on a Si(111) wafer). The samples were selected for flatness with a Fizeau interferometer. Total scattering measurements using an Al $K\alpha$ source (1486.6 eV) have shown roughness values near 4 Å for Si wafers of this type.

Surface cleaning was applied in the following manner: Each sample was placed for 8–12 h on a hot plate (200–250 °C) in O_2-enriched atmosphere and irradiated with UV light emitted from a low-pressure mercury discharge lamp, with an input power of 10 W. The purpose of this step is to remove the organic contamination that exists in the form of hydrocarbons on the surface of the sample. The UV rays from the lamp have two bands at 1849 Å and 2537 Å, which are shown to be important in cleaning. The 1849-Å light dissociates O_2 and produces ozone (O_3). The 2537-Å light initiates photodecomposition of O_3 into O_2 and an activated O atom that reacts with the hydrocarbons on the sample surface and decomposes them into volatile compounds such as H_2O and CO_2. The 2537-Å light is also believed[6] to photosensitize organic contamination and to result in enhanced cleaning rates. The fact that the 1849-Å light (responsible for the creation of O_3) has a low penetration depth in air and the 2537-Å light (responsible for the dissociation of O_3) has a long penetration depth, results in a strong O_3 concentration gradient around the UV source. Thus the cleaning rates are strongly dependent on the lamp distance from the sample, and for the cleaning to be effective samples should be placed not far from the lamp (a distance of ~1 cm was used). The activated O atoms that react to remove the organic contamination from the surface cause, at the same time, further oxidation of the Si surface. However, this side effect is not a problem at this stage of the cleaning procedure because the HF etching step that follows removes the SiO_2 from the surface. The Teflon and glass vessels used during the HF dipping procedure were degreased in a inorganic oxidizer, H_2SO_4 (reagent grade) solution, and then rinsed thoroughly with ultrapure water [$\rho = 18\ \text{M}\Omega$ cm, total organic carbon = 17 ppb (parts in 10^9)]. Each sample was dipped in a 5% HF:ethanol solution for 5–10 min. The solution was prepared by diluting a 50% HF solution (certified particle grade) in ethanol (reagent grade, consisting of 5 vol. of methanol and 100 vol. of 200 proof ethanol). Then the sample was rinsed in ethanol for 30 s and finally dried in N_2 atmosphere for a few seconds. Using ethanol solution rather than an aqueous solution can be advantageous in dissolving the C picked up from storage in plastic containers, thus reducing the total amount of C contamination on the surface.[7] The HF:ethanol solution etches SiO_2 from the surface and then terminates the dangling bonds mainly with H atoms. The H-passivated surface is much more stable toward oxidation compared with a conventional surface, which has many dangling bonds left.[8]

Immediately after the cleaning, a Si sample is loaded into the reflectometer chamber and maintained under vacuum to prevent new oxidation and C contamination of the H-passivated surface. At the same time, witness samples are taken to an x-ray photoelectron spectroscopy (XPS) system, to let us examine the results of the cleaning procedure. Theoretically, if perfect H-passivation of the surface took place (i.e., SiO_2 completely removed and all dangling bonds terminated by H atoms), the surface should be stable against any new oxidation. However, the cleaning is not 100% effective, and there are always

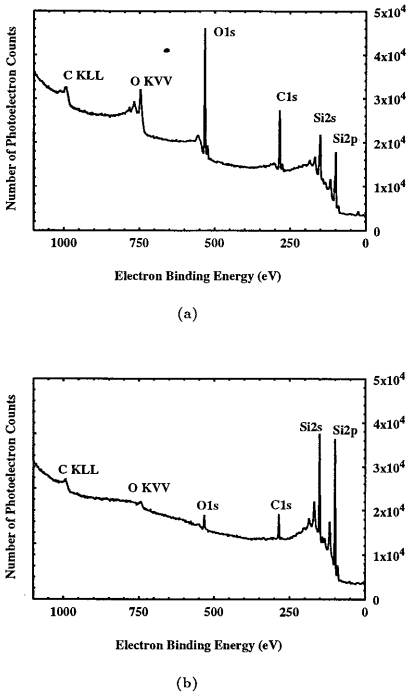

Fig. 2. XPS survey scan results for a Si(111) wafer (a) as received and (b) after H passivation.

remaining dangling bonds or oxidized sites that initiate a slow degradation of the surface. In general the cleaning results highly depend on the amount of organic substance in the atmosphere and also on other undetermined factors such as recontamination from vessels and handling. Surface analysis was performed in a PHI 5300 system at the Lawrence Berkeley National Laboratory, with the XPS method, also known as electron spectroscopy for chemical analysis. A Mg $K\alpha$ source (1253.6 eV) was used in all of the measurements. Typical results are shown in Fig. 2. The peak areas, which represent the integrated photoelectron signal, are proportional to the concentration of an element in the surface region of the sample. From the peak areas the thicknesses of silicon oxide and C on the surface may be calculated,[9] as shown in Table 1. After the cleaning, the samples are usually left with submonolayer (ML) thickness of oxide and ~1 ML thickness of carbon on the surface. Calculations have shown that the effect of this residual contamination in the determination of δ and β is small ($\leq$10%) and is significant only in the low-energy region (below 90 eV). An additional verification of the effectiveness of the H-passivation was performed for an actual reflectance sample at the ALS beamline 6.3.2, as shown in Fig. 3. The electron yield measurements in the oxygen K edge (543.1 eV) energy region show that the oxide is indeed removed after the surface treatment.

B. Instruments

Two instruments were used for the reflectance measurements on the H-passivated Si samples.

Table 1. Overlayer (SiO_2 and C) Thickness Calculations Corresponding to the XPS Results Shown in Fig. 2 for a Si(111) Wafer[a]

Element	Integrated Photoelectron Signal (counts eV/s)	Thickness (Å)	Number of Monolayers (ML)
As received			
Si 2*p*	54,580		
O 1*s*	113,000	7	2.1
C 1*s*	47,127	4.8	5
After H passivation			
Si 2*p*	69,880		
O 1*s*	11,451	0.5	0.2
C 1*s*	14,527	1.1	1.2

[a]The area under the O 1*s* and C 1*s* peaks (integrated photoelectron signal) was used for the oxide and C calculations, respectively.[9] The result for the native oxide (7 Å) on the Si wafer as received is in excellent agreement with values reported in the literature for commercially available Si wafers.[8]

(1) The EUV–soft-x-ray reflectometer is described in detail in Ref. 10. The instrument uses a laser-produced-plasma source and a spherical grating monochromator to produce continuously tunable radiation in the range $30 < E < 300$ eV. The optical components of the monochromator include a cylindrical bent glass premirror; an adjustable aperture (baffle), determining the horizontal beam size; a fixed-line-spacing spherical grating; and an exit slit. Wavelength is scanned by rotation of the grating about an axis parallel to the ruling with a sine bar drive. The exit slit is 12 mm long and has an adjustable width from 10 to 300 μm. After the exit slit, the beam passes through a filter chosen so that it blocks the second harmonic of the wavelength selected by the monochromator. Then the monochromatic light is intercepted by an I_0 detector, which is used to normalize the detected signal and thus eliminate the shot-to-shot noise from the source. Finally, the beam enters the reflectometer

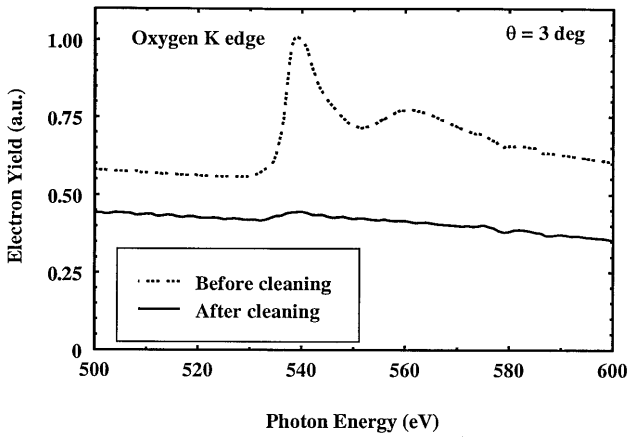

Fig. 3. Electron yield measurements (arbitrary units) on a Si(100) wafer at $\theta = 3°$ (grazing angle), performed at the ALS beamline 6.3.2; before cleaning (dotted curve) there is a pronounced peak at the O K edge (543.1 eV) that is due to the presence of the SiO_2 on the surface; the peak becomes barely visible after surface cleaning (solid curve).

chamber (10^{-5} Torr pressure), where the sample is mounted on a holder (having the ability to rotate and move in three dimensions), and a detector collects the signal after the light has interacted with the sample. The sample position is reproducible to ± 4 μm, and the minimum angle step size is 0.005°. The horizontal beam size at the sample can be varied from 30 mm to less than 1 mm (according to the baffle size), and a vertical beam size of 0.3 mm FWHM has been measured, with the glass mirror focused at the sample. With the full horizontal beam accepted, this system produces 2×10^8 photons/pulse at the output of the monochromator, with 1% bandwidth at 100 eV. The resolving power $E/\Delta E$ of the system varies from 100 to 500, depending on exit slit width and grating aperture. Higher harmonics and stray light have been quantified and are less than 3%. Polarization measurements have shown that the laser plasma source emits unpolarized radiation to at least 95% in intensity, in the energy range of interest for this experiment.

(2) Beamline 6.3.2 at the ALS is described in Ref. 11. This beamline is using radiation from a bending magnet in the energy range $50 < E < 1000$ eV. The optics consist of a plane grating monochromator, a reflectometer chamber (10^{-8} Torr base pressure) and refocusing mirrors to provide a small spot on the sample. The monochromator is an entrance, slitless, varied-line-spacing plane grating design in which the grating operates in the converging light from a spherical mirror working at high demagnification. Aberrations of the mirror are corrected by the line-spacing variation, so that the spectral resolving power $E/\Delta E$ is limited by the ALS source size to ~7000. Energy is scanned by a simple rotation of the grating with a fixed exit slit. The reflectometer has the capability of positioning the sample to ± 4 μm and setting its angular position to 0.002°. The higher harmonics and stray light are suppressed to better than 1% by a combination of filters and a triple reflection low-pass filter. An I_0 detector (measuring the current from the refocusing mirror or the signal from a Au mesh positioned before the reflectometer) is used to normalize the signal against the storage ring current decay. With the full beam accepted, the output photon flux of the monochromator is 10^{12} photons/s into a 0.1% bandwidth at 100 eV. Radiation emitted from beamline 6.3.2 is *s* polarized to at least 90% in intensity, depending on the exact position and size of the vertical aperture at the entrance of the beamline with respect to the beam and on the energy of operation at the ALS (1.5 or 1.9 GeV).

4. Results

A. Discussion of the Reflectance Data

Reflectance measurements on the H-passivated silicon surfaces were performed with the instruments described in Subsection 3.B. Data were collected in the form of reflectance curves $R_{\exp}(\theta)$ for a number of energies in the region 50–180 eV. The software of the instrument allowed for two-dimensional scans; thus, R versus θ scans were performed for a large number of closely separated energy points (0.5 or 1 eV steps). The experimental curves were fitted by means of a least-squares fitting algorithm with the Fresnel equations for the reflected field intensities:

$$R_s(\theta) = \left| \frac{\sin(\theta) - [(1 - \delta + i\beta)^2 - \cos^2(\theta)]^{1/2}}{\sin(\theta) + [(1 - \delta + i\beta)^2 - \cos^2(\theta)]^{1/2}} \right|^2, \quad (7)$$

where θ is measured from the sample surface, $R_s(\theta)$ is the reflectance for *s*-polarized light, and

$$R_p(\theta) = \left| \frac{(1 - \delta + i\beta)^2 \sin(\theta) - [(1 - \delta + i\beta)^2 - \cos^2(\theta)]^{1/2}}{(1 - \delta + i\beta)^2 \sin(\theta) + [(1 - \delta + i\beta)^2 - \cos^2(\theta)]^{1/2}} \right|^2, \quad (8)$$

where $R_p(\theta)$ is the reflectance of *p*-polarized light. The algorithm determines the best-fitted δ and β according to the least-squared error:

$$S = \sum_{i=1}^{N} \frac{[R_{th}(\theta_i) - R_{\exp}(\theta_i)]^2}{{\sigma_i}^2}, \quad (9)$$

where $R_{th}(\theta_i)$, for the theoretical reflectance calculations $[R_{th}(\theta_i) = 1/2[R_s(\theta_i) + R_p(\theta_i)]/2$, was used for the laser-plasma-source measurements and $R_{th}(\theta_i) = R_s(\theta_i)$ was used for beamline 6.3.2); N is the number of angles considered; and σ_i is the (Gaussian) noise for the experimental data $R_{\exp}(\theta_i)$ ($\theta_{\min} \le \theta_i \le \theta_{\max}$, in 1° steps). At the laser-plasma-source reflectometer the sources contributing to ${\sigma_i}^2$ were Poisson noise and electronic noise from the detector (Si photodiode), resulting in an expression of the form ${\sigma_i}^2 = c_1 {R_{\exp}}^2(\theta_i) + c_2$. The parameters c_1 and c_2, were determined separately for each energy and had values of $\sim 10^{-4}$. Thus only data with $R_{\exp}(\theta_i) \ge 1\%$ were used, meaning that the $\theta_{\max}$ considered in each θ scan was between 8° and 20°, depending on the energy. At the ALS the dominant source of noise was electronic noise, which yielded $10^{-5} \le c_1, c_2 \le 10^{-4}$, thus making it possible to use data with $R_{\exp}(\theta_i) \ge 0.3\%$, corresponding to $\theta_{\max}$ in the range 15°–35°. All angle scans started at $\theta_{\min} = 1°$ as a result of the incident photon beam's overilluminating the sample at grazing angles ≤1°.

The (δ, β) values provided after the fitting procedure are shown in Fig. 4. The results look smooth for a range of energies well below the edge, while for the rest of the energies the (δ, β) points look noisy and fluctuating. This behavior is better illustrated in Fig. 5, where contour plots of the statistic S of Eq. (9) are drawn in (δ, β) parameter space for a few energies chosen from the data that were fitted to generate Fig. 4. Each contour area is enclosing the (δ, β) pairs determined by the algorithm with 68% probability of being the true values (68% confidence region) according to the ${\chi_2}^2$ criterion.[2,12] It can be also shown[12] that these contour areas include the true values of the optical constants within $\pm 1\sigma$ error. The two optical constants δ and β are regarded as independent in this parameter estimation model.[12] Figure 5

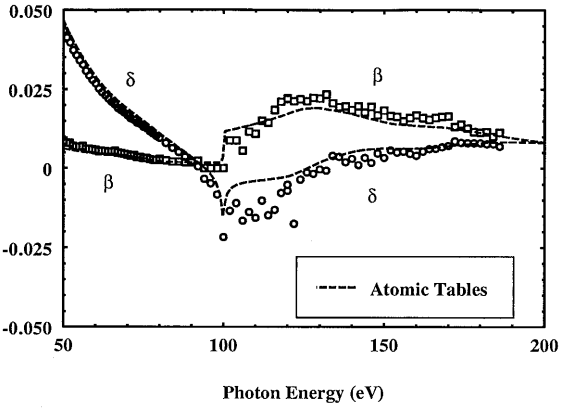

Fig. 4. Optical constants δ (○) and β (□) for a Si(100) sample measured at the ALS beamline 6.3.2. The values for δ and β (dashed curve) from the atomic tables[1] are also shown.

shows that, for the energies well below the edge, the confidence regions are small, indicating that the fitting determines the optical constants with a high degree of certainty (corresponding to the region in Fig. 4 where the data look smooth), whereas for energies close to the $L_{2,3}$ edge and above, the contour areas become quite extended, indicating that the fitting is not reliable (leading to the region of fluctuating data in Fig. 4). For instance, in Fig. 6 the reflectance curves are calculated for two distant (δ, β) pairs inside the 105-eV confidence region (points 105H, 105L, in Fig. 5), and the experimental reflectance data are superimposed. All three curves look similar, which explains why the experimental data could be fitted to any of the two points 105H, 105L or to any other point inside the confidence region. Nevertheless, the large extent of the 105-eV confidence region indicates that the results of the fitting at this

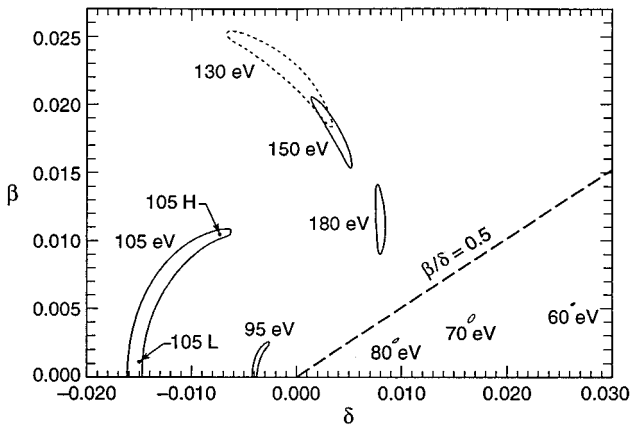

Fig. 5. Contour plots of S generated with data on a Si(100) sample measured at the ALS. The energies shown are 60, 70, 80, 95, 105, 130, 150, and 180 eV in a δ–β axis system. Each contour area encloses the optical constant pairs fitted by the least-squares algorithm within $\pm 1\sigma$ of their true values. This is equivalent to drawing the contours containing (δ, β) fitted with $S \leq S_{\min} + 2.3$, where $S_{\min}$ is the least-squared error, at each energy.[2,12] The line $\beta/\delta = 0.5$ indicates the boundary between regions of reliable and uncertain fitting.

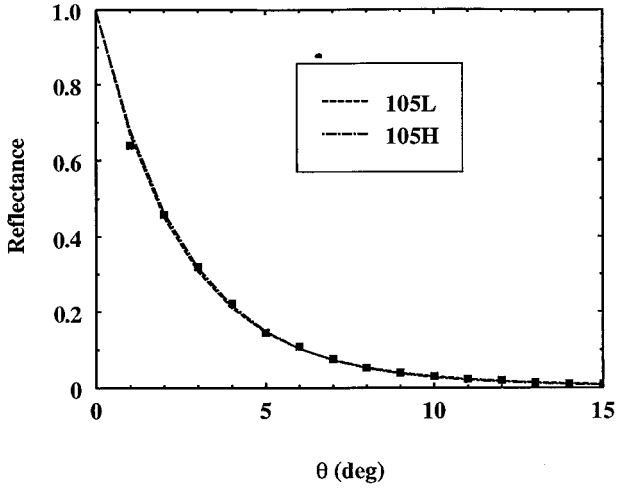

Fig. 6. Reflectivity curves calculated for s-polarized light and with $\delta = -0.00725$, $\beta = 0.0105$, shown as point 105H in Fig. 5 and with $\delta = -0.015$, $\beta = 0.001$, shown as point 105L in Fig. 5. The reflectance data at 105 eV for a Si(100) sample measured at the ALS beamline 6.3.2 are also shown.

energy cannot be used to determine both δ and β accurately. This behavior of the fitting algorithm can be related to the shape of the reflectance curves at different energy regions, which depends on β/δ. Figure 7 shows calculated reflectances for a number of β/δ values. For $\beta/\delta \ll 1$ the reflectance curves have a well-defined shoulder, whereas as β/δ approaches 1 the curves become exponentiallike (negative δ values also result in exponentiallike reflectance curves). Obviously, the fitting is successful for energies with β/δ sufficiently below 1, while for $\beta/\delta \sim 1$ or $\delta < 0$ the results for the optical constants are not reliable. This behavior is inherent to the shape of $R(\theta)$, which depends only on β/δ. Therefore it should not be unique to Si or this particular energy range. For instance, Hunter[13] has observed, by means of isoreflectance curves, a correlation between the sensitivity of the reflectance method and the real and the imaginary parts of n.

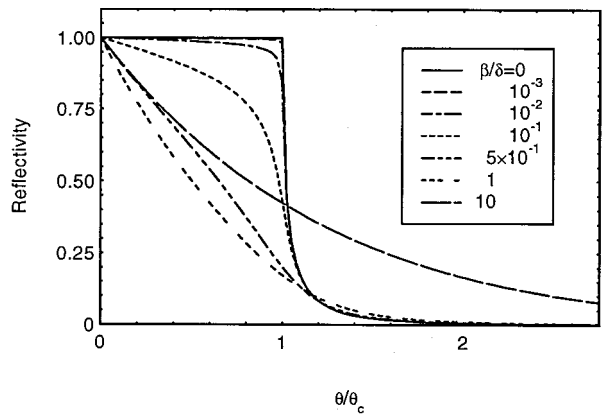

Fig. 7. Calculated reflectivity curves for s-polarized radiation and a range of β/δ values. On the horizontal axis the grazing angle (θ) is normalized to the critical angle $\theta_c = \sqrt{2\delta}$.

For the case of Si, it is demonstrated in Fig. 5 that the region in δ–β space where $\beta/\delta \leq 0.5$ (corresponding to energies ≤90 eV) may be chosen as a conservative guide for a region with reliable fitting results. However, the value $\beta/\delta = 0.5$ is not rigorous and certainly depends on experimental conditions such as noise and photon flux, which may vary for different measurements.

The effect of residual contamination on the sample surface after the H-passivation procedure (discussed in Subsection 3.A) was taken into account in the fitted values of the optical constants, and a correction was applied each time. In the range 50–90 eV, for submonolayer oxide and ≃1 ML organic contamination (typical amounts of residual contamination), the correction for δ was $\pm 1 - 2\%$, and β was overestimated by less than 10%. Separate calculations and corrections were made for each sample, according to the surface analysis results for the residual thicknesses.

It should be noted that reflectance values in the EUV–soft-x-ray range are sensitive to the state of polarization of the photon beam and the roughness of the sample surface. Previous researchers[2,3] have used polarization and roughness as adjustable parameters in addition to δ and β in the fitting model. The analysis presented above assumes a known state of polarization of the source and perfectly flat and smooth samples. Radiation from the laser plasma source has been assumed to be unpolarized, and the ALS beamline 6.3.2 light has been assumed to be *s* polarized in the fitting model. Both assumptions approximate the true state of the source polarization by at least 90%, as explained in Subsection 3.B. There is small but nonzero roughness on the sample surface (see Subsection 3.A), which has not been taken into account in the fitting of the present reflectance data. This choice was made after it was noticed how sensitive the fitting algorithm is with only two adjustable parameters (δ and β). Introduction of a third parameter would make the confidence regions larger, thus introducing greater uncertainty in the fitting results. Calculations have shown that the presence of a possible correction in the state of polarization of the source (≤10%) and the effect of surface roughness (≤4 Å) in the fitting algorithm would modify the fitted values of δ and β by less than 0.1% in the range 50–90 eV. Thus, regarding polarization and roughness as fixed parameters in the fitting of the present reflectance data might introduce only a trivial error into the values of the optical constants.

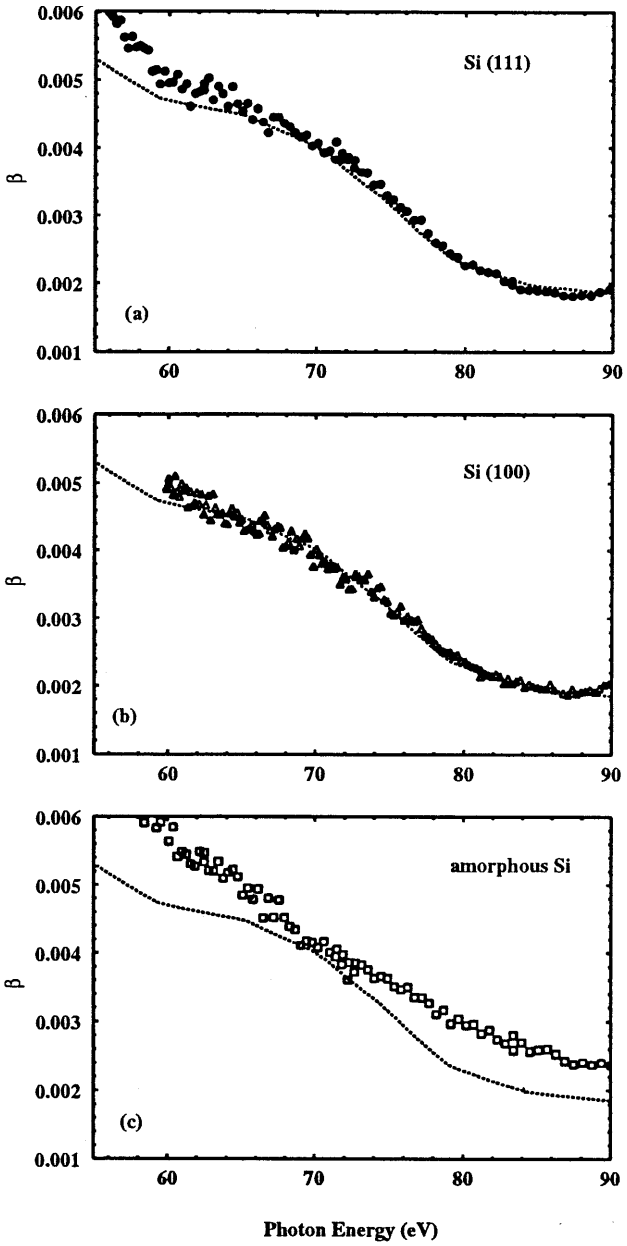

Fig. 8. Fitted values of β determined from reflectance measurements at the laser plasma source for (a) a Si(111) sample, (b) a Si(100) sample, and (c) an amorphous Si sample. Small corrections (≤10%) for the presence of residual contamination were applied for each of the sets of data. The dotted curves represent transmission data for Si(111) presented by Gullikson *et al*. in Ref. 4.

B. Comparison with the Tabulated Values

The derived optical constants of Si will be discussed in the 50–90 eV range only because the fitting algorithm fails to produce reliable results for the rest of the energies considered in this work. It was found that the absorptive part β of the refractive index *n* for crystalline Si exhibits structure in the region 60–80 eV, as shown in Figs. 8(a) and 8(b). This effect was observed for both Si(111) and Si(100) samples and is in agreement with previous transmission data for crystalline Si.[4] It is shown in Fig. 8(c) that the structure is not present in the case of amorphous Si, thus indicating that this effect is probably related to the geometric periodicity of the crystalline Si lattice. Another possibility would be that O was incorporated into the film during deposition. However, by modeling this it does not appear possible to fit the measured β.

In Fig. 9 the measured values of δ are plotted in the energy range 55–90 eV. The values as determined

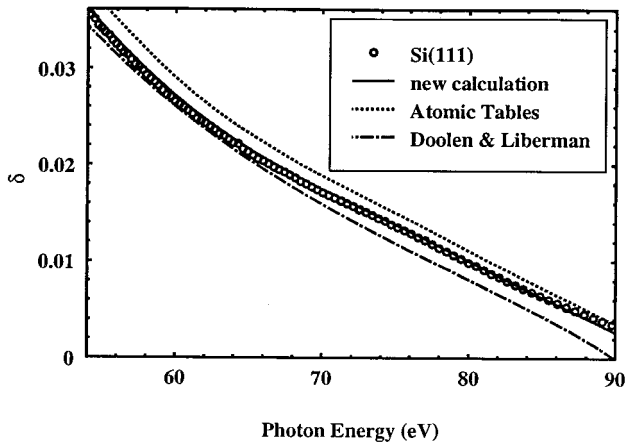

Fig. 9. Fitted values of δ determined from reflectance measurements on a Si(111) sample measured at the laser plasma source in the region 55–90 eV are shown to be in agreement with the Kramers–Kronig calculations for δ (solid curve), by use of absorption data that satisfy the sum rule. Consistent results for δ in this energy range were obtained from measurements of several Si(100) and Si(111) samples by use of both the laser-plasma source and the ALS. The Kramers–Kronig calculations from the tables in Ref. 1 (dotted curve) appear to overestimate the values for δ by 8–15%. Theoretical calculations with a linear response approximation model[15] (dashed–dotted curve) are also shown.

by the Kramers–Kronig relations are shown as a dotted curve. It appears that the Kramers–Kronig method overestimates δ in this region by 8%–15%. As is discussed in Section 2, this is qualitatively consistent with the observed missing oscillator strength in the absorption spectrum. As a further verification, δ was recalculated from the Kramers–Kronig relations with absorption data that satisfied the sum rule in Eq. (5). This was achieved by adjusting the fitted absorption coefficient in the energy region above the silicon $L_{2,3}$ edge (150–300 eV) where the absorption is high. Modifications were made within the error bars of the available experimental data[14] until the sum rule was satisfied. The modified absorption data were also closer to the photoabsorption calculations with the linear response approximation of Doolen and Liberman.[15] As can be seen in Fig. 9, the new Kramers–Kronig calculation is in remarkably good agreement with the present measurements.

5. Conclusions

Reflectance data on the optical constants of crystalline and amorphous Si in the region 50–180 eV are presented in this paper. Surface analysis and photoelectric yield measurements show that a two-step procedure, including UV irradiation and subsequent HF etching of the samples, is successful in removing C contamination and native oxide and in achieving H-passivation of the sample surface. A least-squares fitting algorithm is used to derive the optical constants δ and β from the experimental data; this method is reliable only in regions where β is sufficiently below δ, and produces results with large uncertainties in the energy range in which $\beta \geq \delta$. The effect of the β/δ ratio in the fitting of a reflectance curve has a purely mathematical nature; thus the above reliability criteria should apply to the fitting of reflectance data from any material in any energy range. However, the exact value of β/δ that marks the boundary between reliable and uncertain fitting should depend on the particular experimental conditions, and therefore it has to be determined separately in each case.

In this experiment reliable data are obtained in the range 50–90 eV (below the silicon $L_{2,3}$ edge), corresponding to $\beta/\delta \leq 0.5$. It is shown that crystalline Si exhibits structure from 60 to 80 eV, also observed in previous transmission data. Furthermore, the fitted values for δ are compared with the tabulated values.[1] It is demonstrated through the sum rule that the tabulated values in Ref. 1 should overestimate δ because of missing oscillator strength in the absorption coefficient data used. This effect is verified by the present reflectance results for δ.

The above discussion suggests that least-squares fitting of reflectance data may not be a suitable method for the determination of the refractive index in certain energy regions; different techniques should be explored in the regions for which the fitting algorithm becomes problematic. Particularly for Si, there is a need for improved measurements in the region above the $L_{2,3}$ edge, where the available absorption data are poor and the reflectance method fails to provide reliable results.

The authors are thankful to J. H. Underwood for many stimulating discussions and for his support in carrying out these measurements. We gratefully acknowledge S. Irick, F. Ogletree, and N. Palaio for their contributions in the experimental part of this work. This work was supported by the Advanced Research Projects Agency Advanced Lithography Program and by the Office of Basic Energy Sciences, U.S. Department of Energy, under Contract DE-AC03-76SF00098.

References

1. B. L. Henke, E. M. Gullikson, and J. C. Davis, At. Data Nucl. Data Tables **54** (1993).
2. D. L. Windt, W. C. Cash, Jr., M. Scott, P. Arendt, B. Newnam, R. Fisher, A. B. Swartzlander, P. Z. Takacs, and J. M. Pinneo, "Optical constants for thin films of C, diamond, Al, Si, and CVD SiC from 24 Å to 1216 Å," Appl. Opt. **27,** 279–295 (1988).
3. F. R. Bartsch, H. G. Birken, C. Kunz, and R. Wolf, "Reflectance and total photoelectric yield measurements of silicon wafers in the XUV spectral range," Semicond. Sci. Technol. **5,** 974–979 (1990).
4. E. M. Gullikson, P. Denham, S. Mrowka, and J. H. Underwood, "Absolute photoabsorption measurements of Mg, Al, and Si in the soft-x-ray region below the $L_{2,3}$ edges," Phys. Rev. B **49,** 16283–16288 (1994).
5. D. Y. Smith, "X-ray optical properties: a review of the constraints and the data base," in *X-Ray and Vacuum Ultraviolet Interaction Data Bases, Calculations, and Measurements*, N. K. Del Grande, P. Lee, J. A. Samson, and D. Y. Smith, eds., Proc. SPIE **911,** 86–99 (1988).

6. R. W. C. Hansen, J. Wolske, D. Wallace, and M. Bissen, "Cleaning of optical surfaces with photogenerated reactants," Nucl. Instrum. Methods A **347,** 249–253 (1994).
7. J. M. C. Thornton and R. H. Williams, "S/XPS Study of hydrogen terminated, ordered silicon (100) and (111) surfaces prepared by chemical etching," Phys. Scr. **41,** 1047–1052 (1990).
8. T. Takahagi, I. Nagai, A. Ishitani, and H. Kuroda, "Formation of hydrogen passivated silicon single-crystal surfaces using ultraviolet cleaning and HF etching," J. Appl. Phys. **64,** 3516–3521 (1988).
9. A. F. Carley and M. W. Roberts, "X-ray photoelectron spectroscopic study of the interaction of oxygen and nitric oxide with aluminum," Proc. R. Soc. London Ser. A **363,** 403–424 (1978).
10. E. M. Gullikson, J. H. Underwood, P. J. Batson, and V. Nikitin, "Soft x-ray/EUV reflectometer based on a laser produced plasma source," J. X-Ray Sci. Technol. **3,** 283–299 (1992).
11. J. H. Underwood, E. M. Gullikson, M. Koike, P. J. Batson, P. E. Denham, K. D. Franck, R. E. Tackaberry, and W. F. Steele, "Calibration and standards beamline 6.3.2 at the advanced light source," in *Conference on Synchrotron Radiation Instrumentation '95*, in Rev. Sci. Instrum. **67** (1996), available only on CD-ROM.
12. M. Lampton, B. Margon, and S. Bowyer, "Parameter estimation in x-ray astronomy," Astrophys. J. **208,** 177–190 (1976).
13. W. R. Hunter, "Measurement of optical properties of materials in the vacuum ultraviolet spectral region," Appl. Opt. **21,** 2103–2114 (1982).
14. C. Gähwiller and F. C. Brown, "Photoabsorption near the $L_{II,III}$ edge of silicon and aluminum," Phys. Rev. B **2,** 1918–1925 (1970).
15. G. Doolen and D. A. Liberman, "Calculations of photoabsorption by atoms using a linear response method," Phys. Scr. **36,** 77–79 (1987).